



Transactions of Nonferrous Metals Society of China

www.tnmsc.cn



Trans. Nonferrous Met. Soc. China 33(2023) 3783-3796

# Microstructure and hydrogen storage property of as-milled La-Y-Mg-Ni alloy

Wei ZHANG<sup>1</sup>, Dong-liang ZHAO<sup>1</sup>, Yang-huan ZHANG<sup>1,2</sup>, Shi-hai GUO<sup>1</sup>, Yan QI<sup>1</sup>

Department of Functional Material Research, Central Iron and Steel Research Institute, Beijing 100081, China;
 Collaborative Innovation Center of Integrated Exploitation of Bayan Obo Multi-metal Resources,
 Inner Mongolia University of Science and Technology, Baotou 014010, China

Received 26 May 2022; accepted 9 November 2022

**Abstract:** To improve the hydrogen storage property of La–Y–Mg–Ni alloy, the La<sub>1.7</sub>Y<sub>0.3</sub>Mg<sub>16</sub>Ni alloys with an amorphous and nanocrystalline structure were prepared by ball milling the as-cast alloy for 5–30 h. The effects of microstructure on hydrogen storage property and its mechanism were analyzed. The results show that with prolonging milling time, the crystallinity, grain size and particle size decrease and the amorphous phases increase. The dual regulation of the nanocrystalline and amorphous phases results in the hydrogen storage kinetic property increasing at first and declining later. The 15 h-milled alloy gets the best hydrogenation and dehydrogenation kinetic property, which can absorb 3.10 wt.% hydrogen gas in 10 min at 373 K and has the lowest dehydrogenation activation energy of 71.2 kJ/mol. The thermodynamic property of the alloys milled for different time shows a little change, and the 15 h-milled alloy has the lowest dehydrogenation enthalpy change of 72.9 kJ/mol.

**Key words:** Mg-based alloy; ball milling; microstructure; grain refinement; nanocrystalline; amorphous phase; hydrogen storage kinetics

#### 1 Introduction

Facing the excessive consumption of fossil fuels and environmental pollution, researchers consider vehicles powered by clean and renewable energy as a promising strategy [1]. Hydrogen fuelcell vehicles are considered to be the best solution for transportation. To apply hydrogen widely in portable electronic products and automobiles, developing a safe and suitable hydrogen storage system becomes a crucial step [2]. Owing to the advantages of high density, extensive applicability and high safety, storing hydrogen in hydrides is considered to be a promising hydrogen storage method [3,4].

The borohydrides such as NaBH4 and LiBH4

have high hydrogen storage capacity (>10 wt.%) and can provide hydrogen rapidly by hydrolysis; however, the hydrolysis products are difficult to reabsorb hydrogen. Although a method to regenerate borohydrides by ball milling Mg and hydrolysis products has been found [5-7], the defects of borohydrides, which cannot absorb and desorb hydrogen in cycles, still limit their application. Unlike borohydride, Mg has a good performance of cyclic hydrogen absorption and desorption. Moreover, Mg has many other advantages in storing hydrogen, such as lightweight, large reserves, low cost, innoxious and high hydrogen storage density (~7.6 wt.%) [8]. Researchers have found a lot of countermeasures to overcome the disadvantages of Mg-based alloys, such as high thermal stability, difficulty for activation,

high decomposition temperature and low rates for hydrogen absorption and desorption [9,10]. Mechanical milling of Mg-based alloys with appropriate additives is identified as an effective solution, because the added active sites, reduced particle size, introduced defects and active surfaces will result in the dramatic improvement in hydrogenation and dehydrogenation kinetics [11]. In addition, because Mg has a low melting point (~923 K) and boiling point (~1363 K), many metals with high melting points can hardly alloy with Mg in traditional ways. Ball milling can circumvent this limitation and achieve alloying of Mg with refractory metals [12].

Introducing transition metals is also an effective way to improve the hydrogen storage property of Mg because transition metals can not only decrease the strength of Mg-H bond but also prevent MgH<sub>2</sub> particles from sintering and growing [13]. Transition metals can be introduced in many forms, such as simple substances, oxides, and fluorides [14-18]. OUYANG et al [19-21] dual-tuned the thermodynamics and kinetics of Mg-based alloys by introducing MgF<sub>2</sub> and In and found a significant improvement resulting from plasma milling which can easily prepare nanomaterials. MA et al [22] replaced Mg in CaMg2 with Ni to prepare CaMg<sub>1.9</sub>Ni<sub>0.1</sub> alloy and found that the CaMg<sub>1.9</sub>Ni<sub>0.1</sub> alloy can absorb hydrogen at room temperature and its hydrogenation activation energy is as low as 41.74 kJ/mol. Besides, rare earth elements and their compounds can also be added as catalysts because they can reduce the stability of hydrides and improve the rates of absorbing and desorbing hydrogen [23]. ZHANG et al [24] prepared a nanoscale MgY sample, which has a very low dehydrogenation activation energy of 25.8 kJ/mol and hydrogen desorption enthalpy of 55.9 kJ/mol.

Reducing the particle size of Mg-based alloys is beneficial to improving their hydrogen absorption and desorption rates because of the increased reactive surfaces of alloy particles and the shrunk paths for hydrogen diffusion [25]. In fact, the particle sizes of the as-milled alloy do not always shrink with prolonging milling time, because milling for too long time will result in the aggregation and growth of particles, which will weaken the hydrogen storage performances [26]. In addition, the longer time milling also gives rise to

the formation of an amorphous phase, lowering hydrogen absorption capacity. In the present study, the La<sub>1.7</sub>Y<sub>0.3</sub>Mg<sub>16</sub>Ni alloy was prepared by partly replacing La and Mg in La<sub>2</sub>Mg<sub>17</sub> alloy with Y and Ni, respectively. Ball milling with different milling time was utilized to change the microstructure of the alloy, and the activation property and hydrogen storage thermodynamic and kinetic performances of the as-milled alloys were systematically investigated.

#### 2 Experimental

The La<sub>1.7</sub>Y<sub>0.3</sub>Mg<sub>16</sub>Ni alloy was prepared in a vacuum induction furnace with high-purity (≥99.9%) raw materials of La, Y, Mg and Ni. The smelting process was carried out under the protection of 0.04 MPa helium to prevent Mg from volatilizing. Extra amounts of 5 wt.% La and Y and 8 wt.% Mg were added during the batching to offset the burning loss during smelting. The alloy ingot was mechanically crushed into powders (≤75 µm) before ball milling. The ball milling process was carried out at 350 r/min and a ball-to-powder mass ratio of 40:1. Argon was filled into the ball mill tanks as a protective gas. To make the alloy powders dissipate heat in time for preventing cold welding during the ball milling, the mill was interrupted for 0.5 h after running every 0.5 h. The milling time was 5, 10, 15, 20 and 30 h, respectively. For convenience, the alloys are represented by M<sub>5</sub>, M<sub>10</sub>, M<sub>15</sub>, M<sub>20</sub> and M<sub>30</sub> respectively according to different milling time, and the as-cast alloy is represented by M<sub>0</sub>.

The phase structures and compositions of samples were examined by X-ray diffraction (XRD). The diffraction was performed with Cu  $K_{\alpha l}$  radiation at 160 mA and 40 kV filtered by graphite. The morphology of alloy particles was observed by a scanning electron microscope (SEM). The particle size of the alloys before and after activation was analyzed with a particle size analyzer. The crystalline state and microstructure of the alloys were characterized with a high-resolution transmission electron microscope (HRTEM).

The activation property and hydrogen storage thermodynamics and kinetics of the as-milled alloys were gotten by measuring 500 mg sample alloys in an automatic Sieverts apparatus. Six hydrogen absorption and desorption cycles were carried out at

633 K to activate the samples by absorbing hydrogen under 3 MPa and desorbing hydrogen under  $1\times10^{-4} \text{ MPa}$ . After activation, the enthalpy change ( $\Delta H$ ) of alloys was calculated from the P-C-T (pressure–composition–temperature) curves measured at 593, 613 and 633 K, respectively. The hydrogen absorption property measurement was conducted at 3 MPa and different temperatures of 373, 423, 473, 533, 553, 573, 593, 613 and 633 K, respectively, while the hydrogen desorption performance test was carried out at  $1\times10^{-4}$  MPa and different temperatures of 533, 553, 573, 593, 613 and 633 K, respectively.

#### 3 Results and discussion

#### 3.1 Phase composition and microstructure

Figure 1 depicts the XRD patterns of the La<sub>1.7</sub>Y<sub>0.3</sub>Mg<sub>16</sub>Ni alloys with different milling time before and after hydrogenation dehydrogenation. The ICDD identification of the XRD curves reveals that the alloys are composed of the major phase of La<sub>2</sub>Mg<sub>17</sub> and the second phases of Mg2Ni and La2Ni3. Substituting Y for La does not create a new phase, which means that Y occupies the site of La and forms solid solutions [27]. After hydrogen absorption, four hydrides of MgH<sub>2</sub>, Mg<sub>2</sub>NiH<sub>4</sub>, LaH<sub>3</sub> and YH<sub>2</sub> appear in M<sub>0</sub> alloy. However, the diffraction peaks of YH<sub>2</sub> are difficult to be distinguished in the hydrogenated as-milled alloys. This is because the content of Y in the alloy is low, and the XRD diffraction peaks are broadened after ball milling, which makes it difficult to identify the small peaks of YH<sub>2</sub>. The reactions that occurred in absorbing hydrogen can be inferred as follows based on the phases identified from the XRD curves in Figs. 1(a) and (b):

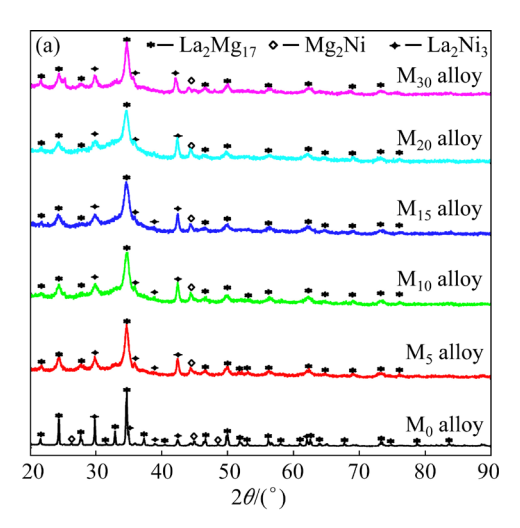
$$La_2Mg_{17}+H_2 \rightarrow LaH_3+MgH_2 \tag{1}$$

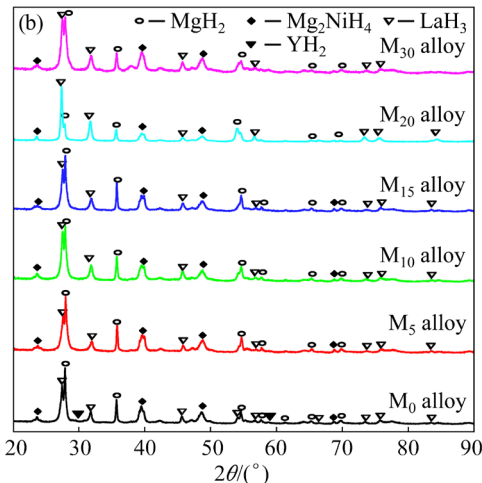
$$Mg_2Ni+H_2 \rightarrow Mg_2NiH_4$$
 (2)

$$La_2Ni_3+La_2Mg_{17}+H_2\rightarrow LaH_3+Mg_2NiH_4+MgH_2$$
 (3)

$$Y+H_2 \rightarrow YH_2$$
 (4)

After desorbing hydrogen, Mg, Mg<sub>2</sub>Ni, LaH<sub>3</sub> and YH<sub>2</sub> phases are distinguished from the XRD curves of Fig. 1(c). Evidently, the LaH<sub>3</sub> and YH<sub>2</sub> phases do not decompose after dehydrogenation owing to their high thermostability. The reactions that occur during the hydrogen desorption process can be drawn as follows:





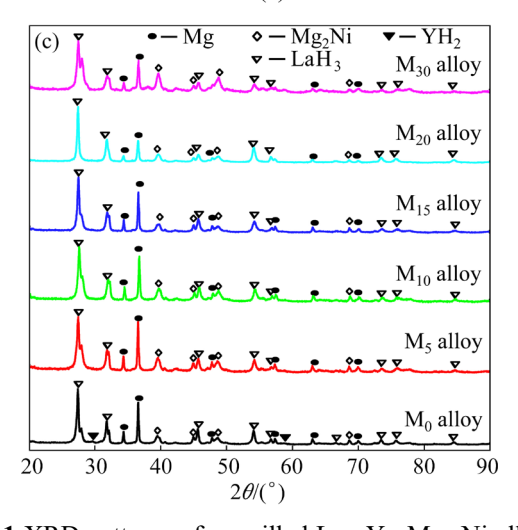


**Fig. 1** XRD patterns of as-milled La<sub>1.7</sub>Y<sub>0.3</sub>Mg<sub>16</sub>Ni alloys: (a) Before hydrogen absorption; (b) After hydrogen absorption; (c) After hydrogen desorption

$$MgH_2 \rightarrow Mg + H_2 \uparrow$$
 (5)

$$Mg_2NiH_4 \rightarrow Mg_2Ni+H_2\uparrow$$
 (6)

From the analysis above, it can be deduced that it is the reversible reactions of  $Mg/MgH_2$  and

Mg<sub>2</sub>Ni/Mg<sub>2</sub>NiH<sub>4</sub> that occur during the absorbing and desorbing hydrogen processes for the activated alloys. The reversible reactions are as follows:

$$Mg+H_2 \longrightarrow MgH_2$$
 (7)

$$Mg_2Ni+H_2 \longrightarrow Mg_2NiH_4$$
 (8)

It can also be observed from Fig. 1 that the diffraction peaks of M<sub>0</sub> alloy after hydrogen absorption and desorption are obviously wider than those before hydrogen absorption. This is because the atomic radius of hydrogen is larger than that of lattice interstitial, resulting in the expansion of the lattice after hydrogen absorption. Although the volume of the unit cell can be contracted and part of the stress can be released after hydrogen desorption, it is difficult to restore the original state. As the number of hydrogen absorption and desorption cycles increases, the lattice stress gradually accumulates and eventually breaks the large grains into smaller ones, even forming an amorphous phase, leading to the broadening of diffraction peaks. As for the as-milled alloys, the diffraction peaks are broadened and some of the diffraction peaks disappear, indicating the appearance of amorphous phases. With milling time prolonging, the broadening of the diffraction peaks became more and more obvious, meaning that ball milling is beneficial to reducing grain size and enhancing the degree of amorphization of the alloy.

To verify the above analysis, the crystallinity and average grain size of the alloys were estimated by fitting the XRD curves with the software of Jade, as shown in Fig. 2. After ball milling, the crystallinity of the alloy decreases significantly, indicating the increase of amorphous phases. The crystallinity of the alloy before activation drops sharply from 98.1% to 66.4% with increasing milling time from 0 to 30 h. After several hydrogen absorption and desorption cycles, the crystallinity increases to more than 95%, which means that the hydrogen absorption and desorption reactions are beneficial to the recrystallization of amorphous phases. However, the crystallinity cannot reach 100%, indicating the existence of amorphous phases, and the increasing tendency of amorphous phase with extending milling time keeps unchanged after hydrogen absorption and desorption reactions. The average grain size of the alloy decreases sharply from 80.5 to 17.2 nm after ball milling for 5 h. Extending the milling time could continue to

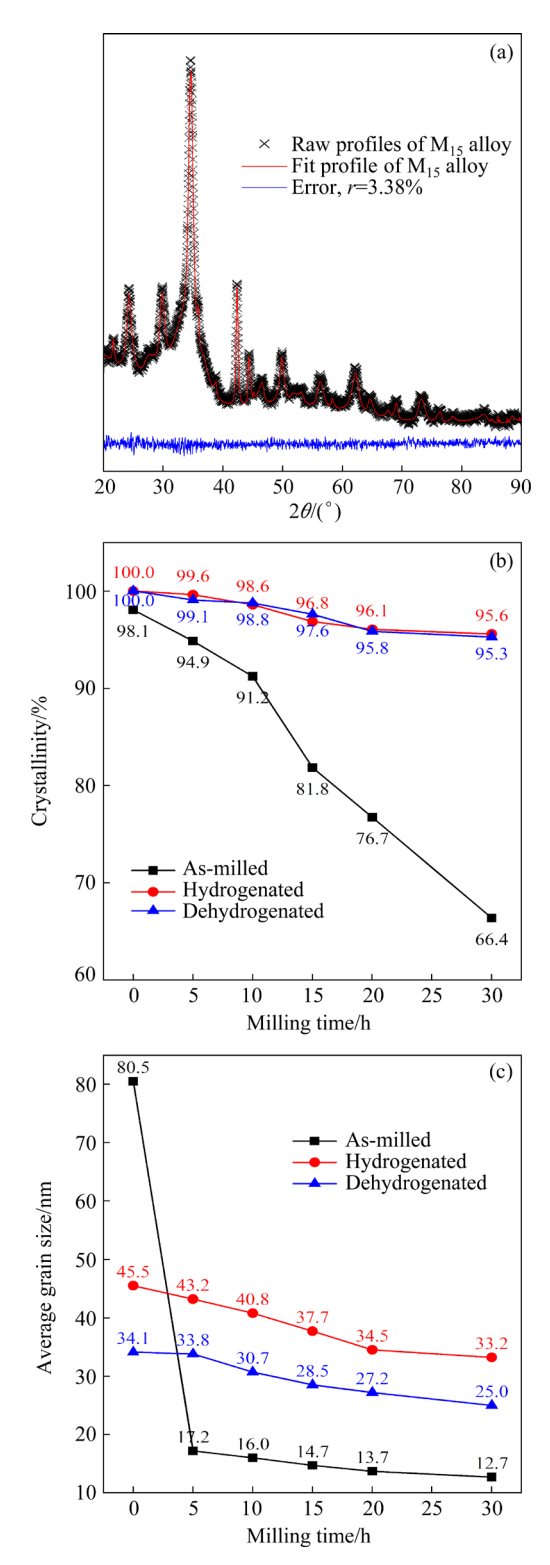


**Fig. 2** Fitting results of alloys from Jade: (a) Fitting results of XRD curves of  $M_{15}$  alloy; (b) Crystallinity of alloys; (c) Average grain size of alloys

reduce the grain size, but the decrease is very small. After multiple hydrogen absorption and desorption cycles, the grain size of alloys increases significantly, owing to the recrystallization during

the processes of absorbing and desorbing hydrogen. Moreover, the grain size of hydrogenated alloys is larger than that of the dehydrogenated alloys, because the volume of hydrides is larger than that of the corresponding alloys [28].

The morphologies of the as-milled (15 and 30 h) La<sub>1.7</sub>Y<sub>0.3</sub>Mg<sub>16</sub>Ni alloy powders before and after activation are exhibited in Fig. 3. The particles are obviously ball-milled powders without obvious edges and corners, and the M<sub>30</sub> alloy has more rounded particles than Mg<sub>15</sub> alloy. After activation, many cracks occur on the particle surface, which is caused by the stress accumulation of the alloy particles during activation. It is well known that the alloy grains expand after hydrogenation and shrink after dehydrogenation. During the whole activation process, the alloy needs to undergo multiple cycles of absorbing and desorbing hydrogen, so that the alloy grains expand and shrink repeatedly, resulting in the continuous accumulation of internal stress on the lattice until a fracture occurs, which makes the alloy particles crack and even pulverize. The particle sizes of alloy powders were measured by a particle size analyzer, and the results are shown in Fig. 4. It shows that the particle size can be decreased through ball milling. With milling time being prolonged from 5 to 30 h, the particle size before activation decreases from 46.0 to  $27.4 \, \mu m$  and the particle size after activation decreases from 38.1 to  $26.3 \, \mu m$ . It is worth noting that with the extension of milling time, the reduction of particle size is lower and lower and the cracks on the surface of activated particles also get less and less. This is because ball milling increases the amorphous phase in the alloy, which acts as a buffer for internal stress and reduces the occurrence of cracks and pulverization.

Figure 5 shows the HRTEM images and selected area electron diffraction (SAED) patterns of the 15 h- and 30 h-milled La<sub>1.7</sub>Y<sub>0.3</sub>Mg<sub>16</sub>Ni alloys before and after absorbing and desorbing hydrogen. An amorphous and nano-crystalline structure can be seen in the as-milled alloys. The comparison of Figs. 5(a) and (d) shows that extending milling time reduces the grain size and increases the amount of amorphous phase, consistent with the result of Fig. 2. After absorbing and desorbing hydrogen, the as-milled alloys keep displaying an amorphous and nanocrystalline structure and proportion amorphous decreases. Consistent with the XRD detection, three hydrides of MgH2, Mg2NiH4 and LaH<sub>3</sub> can be detected in the alloys after hydrogenation, and Mg, Mg<sub>2</sub>Ni and LaH<sub>3</sub> can be found in the hydrogenated alloys, supported by the

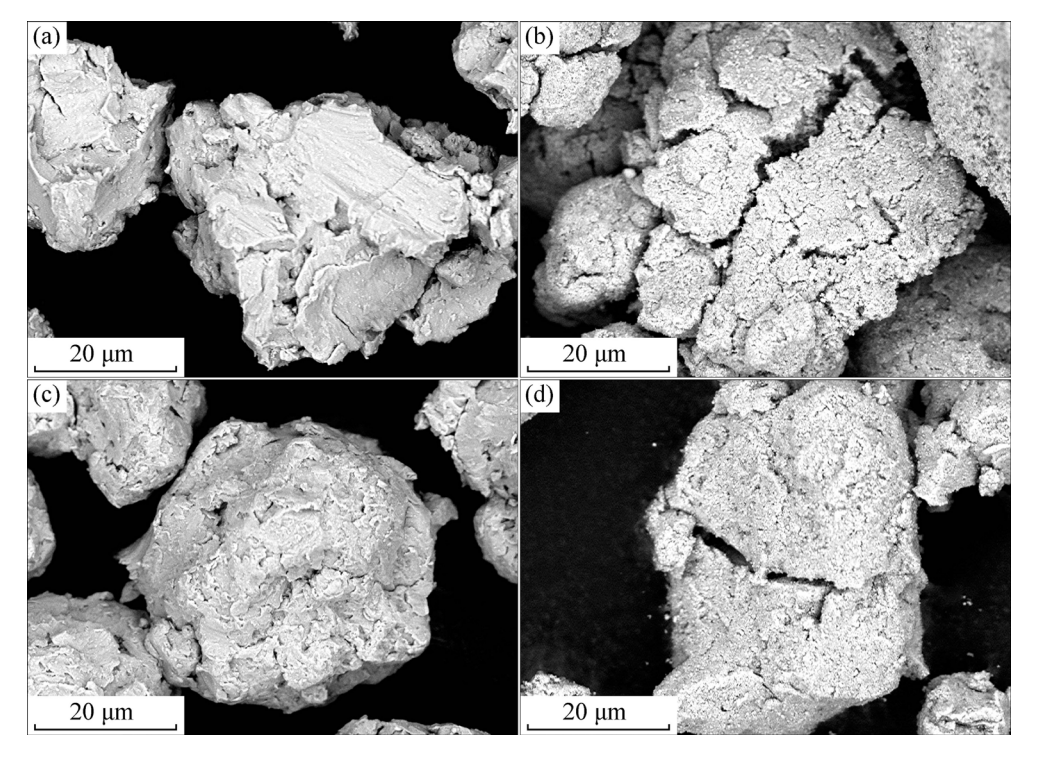


Fig. 3 SEM images of as-milled alloys: (a)  $M_{15}$  before activation; (b)  $M_{15}$  after activation; (c)  $M_{30}$  before activation; (d)  $M_{30}$  after activation

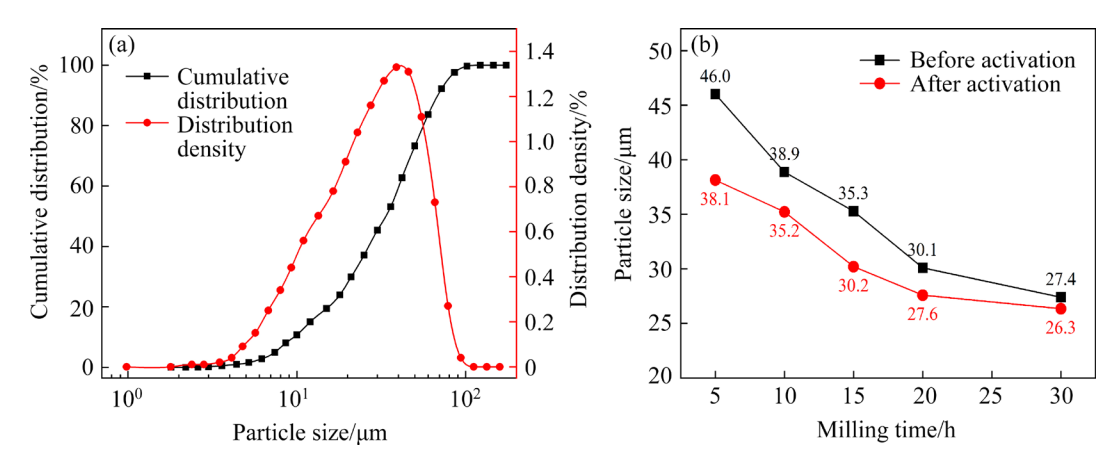


Fig. 4 Particle size of as-milled alloys: (a) Particle size distribution of M<sub>15</sub> before activation; (b) Particle size of alloys

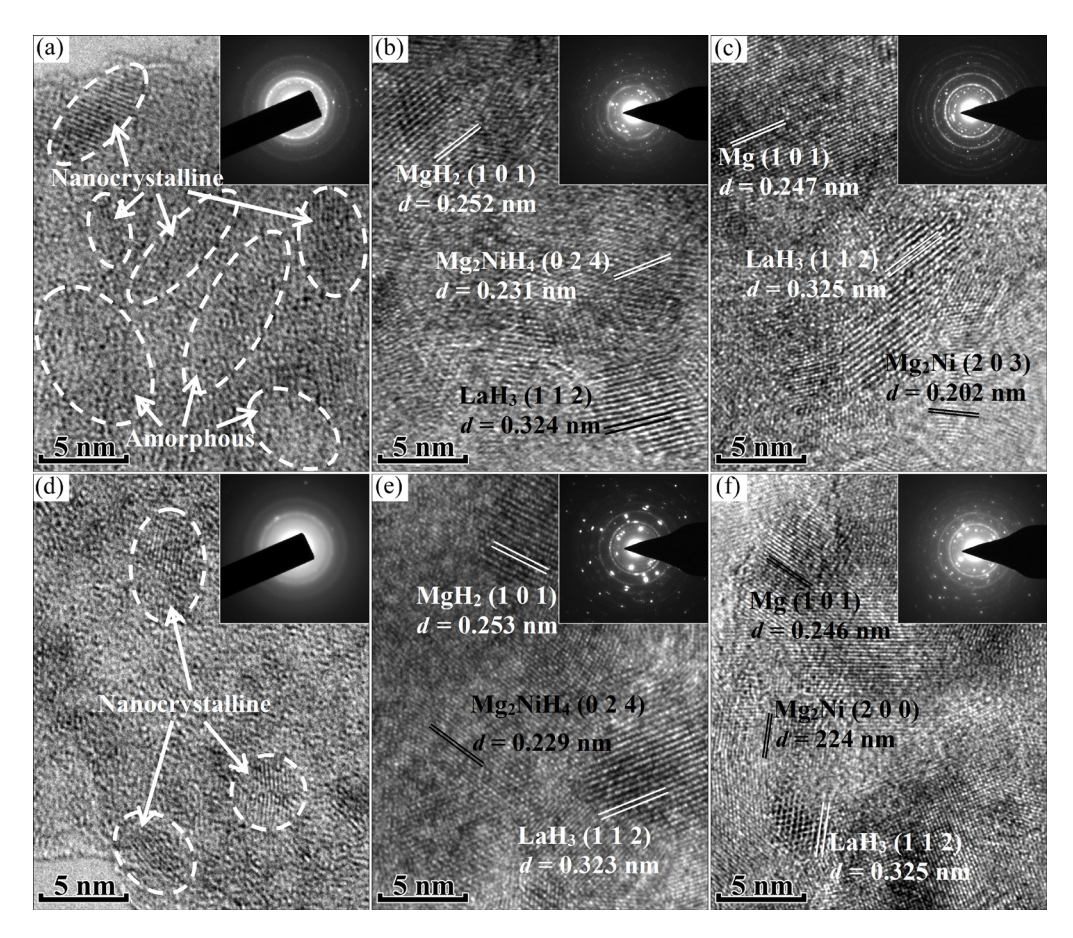


Fig. 5 HRTEM images and SAED patterns of  $M_{15}$  and  $M_{30}$  alloys: (a)  $M_{15}$  before hydrogenation; (b)  $M_{15}$  after hydrogenation; (c)  $M_{15}$  after dehydrogenation; (d)  $M_{30}$  before hydrogenation; (e)  $M_{30}$  after hydrogenation; (f)  $M_{30}$  after dehydrogenation

SAED patterns as well. Apparently, YH<sub>2</sub> phase can hardly be seen because of its low content, and LaH<sub>3</sub> phase does not decompose during hydrogen desorption. Moreover, various crystal defects appear in the HRTEM images, which will provide fast channels for the diffusion of hydrogen inside the alloy.

#### 3.2 Activation property

Activation is an inevitable process for Mg-based alloys, during which the hydrogen storage kinetic property can be improved after several absorbing and desorbing hydrogen cycles. The fewer the cycle number is, the better the activation property of the alloy is. The activation

processes of the as-milled La<sub>1.7</sub>Y<sub>0.3</sub>Mg<sub>16</sub>Ni alloys were carried out at 633 K. Figure 6 presents the isothermal hydrogen absorption and desorption curves during the activation process. It is evident that the hydrogen absorbing and desorbing rates in the first cycle have an obvious variation with milling time. With prolonging milling time from 5 to 10, 15, 20, and 30 h, the time needed for the alloy to absorb 4.00 wt.% hydrogen in the first cycle is 13920, 12960, 12720, 13560 and 17280 s, and the time needed for the alloy to desorb 4.00 wt.% hydrogen in the first cycle is 198, 168, 156, 186 and 216 s, respectively (Figs. 6(a) and (c)). The alloy has the fastest hydrogen absorption and desorption rates after milling for 15 h, and further extending milling time will impair these rates. It is believed that the modified structure in the alloy after ball milling is responsible for the changes in the activation property. A part of the crystal structure in the alloy will be disordered after ball milling, forming a nanocrystalline or amorphous structure, and some new grain boundaries and defects appear in the alloy, which facilitates the hydrogen diffusion inside the alloy by providing lots of sites with low diffusion activation energy [29]. Unfortunately, after milling for more than 15 h, the crystallinity becomes too low and excessive amorphous appears in the alloy, as the diffusion rate of hydrogen atoms in an amorphous phase is slower than that in a nanocrystalline, the activation performance of the alloy begins to decrease.

The time needed for the alloy to reach saturation for hydrogen absorption in the first cycle is much longer than that for the subsequent hydrogen absorption processes (Fig. 6(b)), because there is a thin oxide layer covering the alloy particles before the hydrogen absorption in the first cycle. FRIEDRICHS et al [30] reported that an oxide layer is formed unavoidably on the Mg surface during an experiment, and even under the protection of inert gas, an oxide layer with a thickness of 3–4 nm will also be formed. CHEN et al [31] focused on the oxygen coverage on the Mg (0001) surface and found that the H<sub>2</sub> dissociation and H

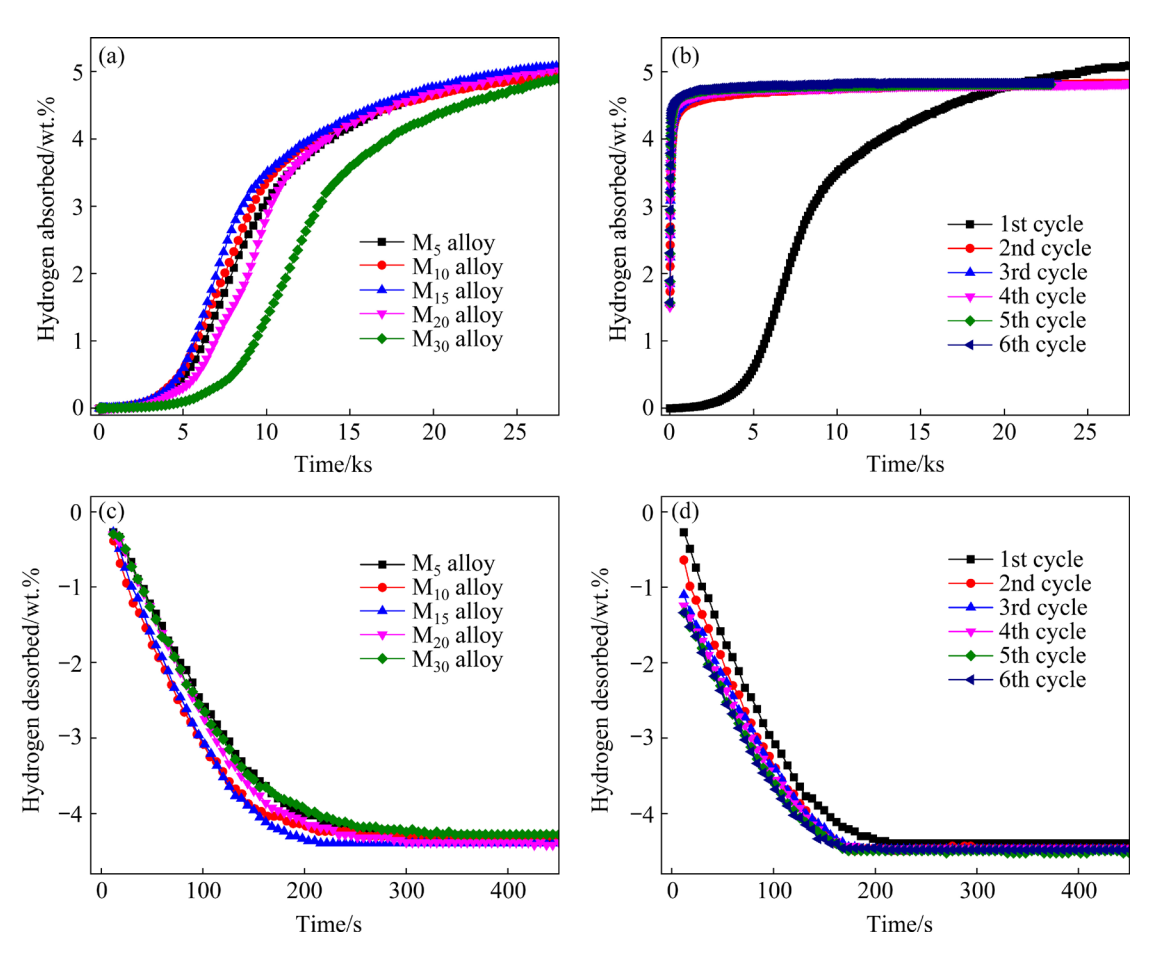


**Fig. 6** Isothermal hydrogen absorption and desorption curves of as-milled La<sub>1.7</sub>Y<sub>0.3</sub>Mg<sub>16</sub>Ni alloy at 633 K: (a) Hydrogen absorption curves in the first cycle; (b) Hydrogen absorption curves of M<sub>15</sub> alloy for activation; (c) Hydrogen desorption curves in the first cycle; (d) Hydrogen desorption curves of M<sub>15</sub> alloy for activation

atom penetration are the rate-limiting steps for the hydrogen absorption at low and high oxygen coverages, respectively. During the hydrogen absorption in the first cycle, hydrogen needs to dissociate first and then pass through the oxide layer, which slows down the hydrogen absorption rate greatly. After completing the first absorbing hydrogen process, the oxide layer breaks up, leading to a significantly faster hydrogen absorption rate in the subsequent cycles. Unlike hydrogen absorption, the hydrogen desorption rate in the first cycle is not much slower than the subsequent hydrogen desorption rates (Fig. 6(d)), which is also due to the destroyed oxide layer when absorbing hydrogen in the first cycle. Furthermore, the hydrogen absorption capacity for the first cycle is higher than that for the subsequent cycles because the generated LaH<sub>3</sub> and YH<sub>2</sub> in the first cycle of hydrogen absorption are difficult to decompose under experimental conditions.

After 6 cycles of absorbing and desorbing hydrogen, the hydrogen absorption and desorption curves are basically overlapped, implying the completion of activation. Because of the augment of amorphous phase with milling time prolongation from 5 to 10, 15, 20, and 30 h, the hydrogen absorption and desorption capacities decrease gradually, which are 4.91, 4.87, 4.85, 4.81 and 4.75 wt.% for the hydrogen absorption capacity and 4.57, 4.54, 4.48, 4.43 and 4.38 wt.% for the hydrogen desorption capacity, respectively.

#### 3.3 Hydrogen storage thermodynamic property

The P-C-T curves of the activated alloys at 593, 613 and 633 K were measured for investigating the influence of microstructure on the hydrogenation and dehydrogenation thermodynamics, as illustrated in Fig. 7. Each P-C-Tcurve has two pressure platforms, both of which decline with the decrease of temperature. The longer and lower platform corresponds to the composition and decomposition of MgH2, and the shorter and higher platform represents reversible hydriding and dehydriding reactions of Mg<sub>2</sub>Ni/Mg<sub>2</sub>NiH<sub>4</sub>. It is noted that the longer pressure platforms are quite flat with very small hysteresis. Based on the plateau pressures of P-C-T curves, the enthalpy change  $(\Delta H)$  of hydrogenation and dehydrogenation reactions can be derived with the Van't Hoff equation [32]:

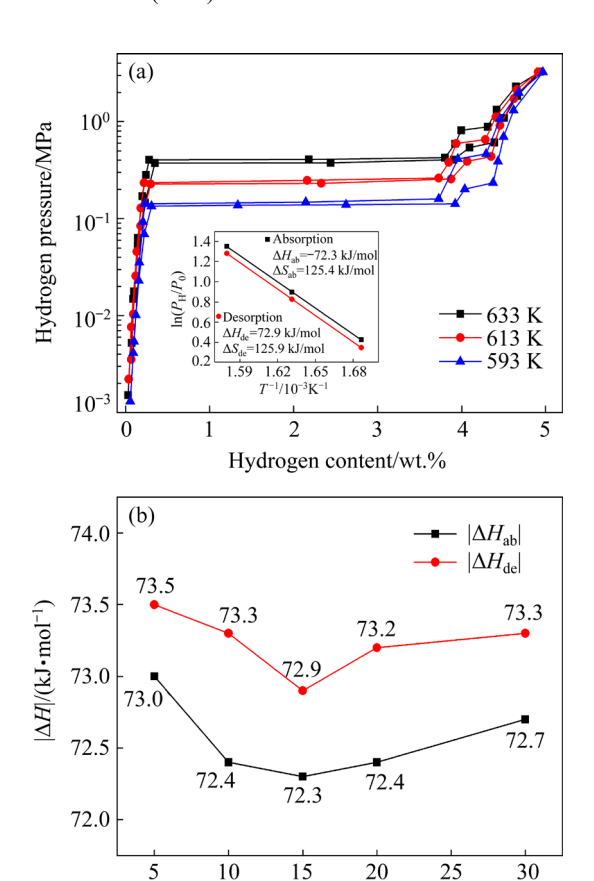


**Fig. 7** P-C-T curves and Van't Hoff plots (a) and enthalpy change of hydrogen absorption and desorption (b) M<sub>15</sub> alloys of M<sub>15</sub> alloy

Milling time/h

10

$$\ln\left(\frac{P_{\rm H}}{P_{\rm o}}\right) = \frac{\Delta H}{RT} - \frac{\Delta S}{R} \tag{9}$$

where  $P_{\rm H}$  is the equilibrium hydrogen pressure (the pressure of the longer platform of Mg/MgH2 was chosen as  $P_{\rm H}$  value);  $P_0$  represents the standard atmospheric pressure;  $\Delta H$  and  $\Delta S$  symbolize the enthalpy and entropy changes of reactions, respectively; R is the molar gas constant; T is the reaction temperature.

The inset in Fig. 7(a) shows the Van't Hoff plot of  $ln(P_H/P_0)$  vs 1/T of  $M_{15}$  alloy which is clear in linear relationships. The  $\Delta H$  value of hydrogenation and dehydrogenation reactions can be calculated from the slope of the fitting line of Van't Hoff plot. Figure 7(b) describes the dependence of the absolute value of  $\Delta H$  on milling time. Extending the milling time from 5 to 30 h results in the absolute value of  $\Delta H$  decreasing at first and increasing later, and the 15 h-milled alloy (M<sub>15</sub>) reaches the lowest points, indicating that the appropriate milling time can improve

the hydriding and dehydriding thermodynamics. The dehydrogenation enthalpy change of M<sub>15</sub> is 72.9 kJ/mol, which is lower than that of pure MgH<sub>2</sub> (79.1 kJ/mol) [19], Mg<sub>3</sub>La hydride (81 kJ/mol) [16] and Ca<sub>5</sub>Mg<sub>9</sub>H<sub>28</sub> (94.8 kJ/mol) [22], and higher than that of plasma-milled Mg(In)-MgF2 composite (69.2 kJ/mol) [20] and Mg<sub>2</sub>In<sub>0.1</sub>Ni hydride (38.4 kJ/mol) [21]. It is reported that the thermodynamics of hydrogenation and dehydrogenation reactions can be improved by introducing capillarity effect when ball milling reduces the particle size to a small enough size, especially to the nanoscale [33,34]. However, the improvement of the hydrogen storage thermodynamics is very limited in this experiment, because the particle size of the as-milled alloys is more than 20 µm, which is much larger than the nanometer size.

#### 3.4 Hydrogen absorption kinetic property

The hydrogen absorption curves of the La<sub>1.7</sub>Ce<sub>0.3</sub>Mg<sub>16</sub>Ni alloy milled for different time were tested at different temperatures from 373 to 633 K, as exhibited in Fig. 8(a). The hydrogen absorption capacity grows quite fast at the beginning stage which can reach more than 90% of saturated capacity within 60 s except 423 and 373 K, while it takes a very long time for the hydrogen absorption capacity to reach saturation in the subsequent stage. This characteristic of the hydrogen absorption curves is related to the rapidly formed hydride layer on alloy surface, which hinders the hydrogen atoms from diffusing into the alloy. The hydride layer will completely block the diffusion of hydrogen into the alloy when its thickness reaches 100 nm, as reported by FRIEDLMEIER and GROLL [35].

Figure 8(b) exhibits the dependence of hydrogen absorption capacity of alloys in 10 min (symbolized by  $C_{10}$ ) with milling time at different temperatures. It can be found that the  $C_{10}$  values are very high with no significant difference when the temperature is higher than 473 K. When the temperature declines to 423 K and below, the  $C_{10}$  value decreases dramatically and a significant difference appears with changing milling time. When absorbing hydrogen for 10 min, the hydrogen content of the alloys shows a trend of increasing at first and decreasing later with milling time prolonging. It is obvious that the  $M_{15}$  alloy has the fastest hydrogen absorption rate at low temperatures,

which can absorb 3.10 wt.% hydrogen in 10 min at 373 K. The  $C_{10}$  values of the  $M_{15}$  alloy and some other alloys are listed in Table 1.

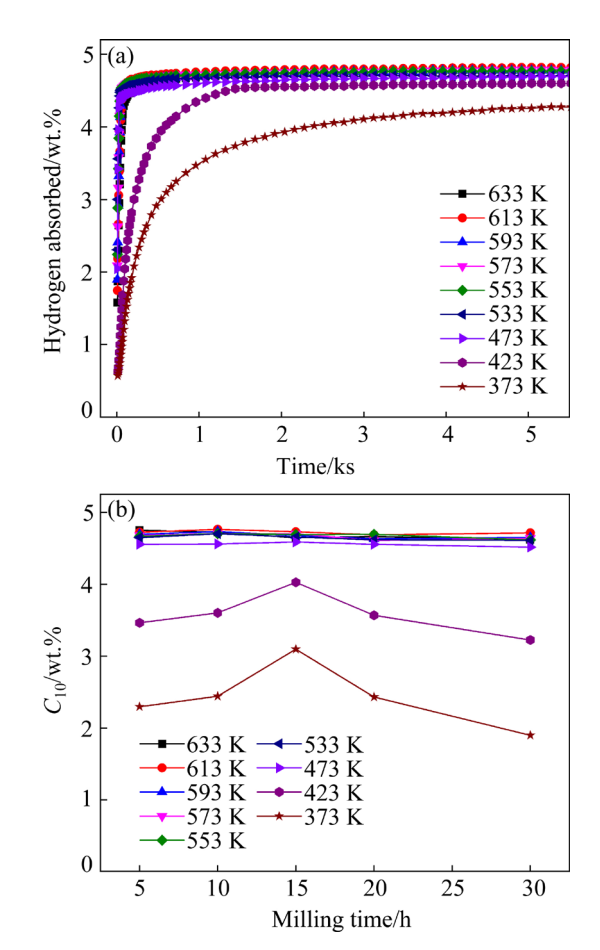


**Fig. 8** Hydrogen absorption curves (a) and hydrogen absorption capacity  $C_{10}$  (b) of  $M_{15}$  alloys

**Table 1** Hydrogen absorption capacities of different alloys in 10 min

Alloy	T/K	C <sub>10</sub> / wt.%	Ref.
MmNi <sub>3.5</sub> (CoMnAl) <sub>1.5</sub> – 30 wt.% Mg	353	0.82	[25]
MmNi <sub>3.5</sub> (CoMnAl) <sub>1.5</sub>	353	1.13	[25]
$PrMg_3Ni_{0.1}\\$	298	1.8	[15]
$PrMg_3$	298	2.0	[15]
$Mg_{80}Ce_{18}Ni_2 \\$	298	2.4	[36]
$LaMg_3Ni_{0.1}$	298	2.7	[16]
$LaMg_3$	298	2.8	[16]
$15 \text{ h-milled } La_{1.7}Y_{0.3}Mg_{16}Ni$	373	3.10	This work
$CeMg_{1.9}Ni_{0.1}$	353	3.2	[22]
MgH <sub>2</sub> -5 mol% Li <sub>2</sub> CO <sub>3</sub>	373	3.8	[37]
MgH <sub>2</sub> -5 wt.% nfTa <sub>2</sub> O <sub>5</sub>	373	5.1	[38]

The change in hydrogen absorption rate with milling time is thought to be related to the proportion of amorphous and nanocrystalline in the alloy. Usually, the hydrogen absorption process of an alloy can be split into three steps: (a) hydrogen molecules dissociating into hydrogen atoms on alloy surface; (b) hydrogen atoms diffusing inside the particles; (c) hydrogen atoms reacting with the alloy and forming metal hydrides [39]. Among the three steps, Step (a) is the rate-controlling factor owing to the high energy needed [40]. Ball milling causes an increase in internal stresses in the alloy, generates new defects inside and on the surface of the particles, reduces the grain size and forms an amorphous and nanocrystalline structure. The lattice defects introduce many active sites with low activation energy, which accelerates the dissociation of hydrogen in Step (a) and the diffusion of hydrogen atoms in Step (b). The smaller particle size shortens the hydrogen diffusion length and increases the reaction surface, which helps to accelerate the hydrogen absorbing and desorbing rates [41]. However, for the amorphous phase, hydrogen can only diffuse on its surface but not inside it. When there are too many amorphous phases, the diffusion of hydrogen atoms will be hindered. After ball milling for an appropriate time, the grains in the alloy are broken into nanocrystals and a small number of nanocrystals are broken into amorphous phases under the action of stress. The promotion effect of nanocrystals on the hydrogen absorption kinetics is greater than the inhibition effect of the amorphous phase, resulting in an increase in the hydrogen absorption rate. However, when the alloy is milled for too long time, it will contain too many amorphous phases, and the hindering effect of amorphous phases on hydrogen diffusion is dominant so that the hydrogen absorption rate begins to slow down.

## 3.5 Hydrogen desorption kinetics and dehydrogenation activation energy

The hydrogen desorption curves of the alloys milled for different time were measured at different temperatures, as presented in Fig. 9(a). The reaction temperature affects the hydrogen desorption kinetics obviously and the hydrogen desorption rate keeps decreasing with the decline of temperature. The time required for an alloy to desorb 3 wt.% hydrogen was symbolized by  $t_3$ , and the values of

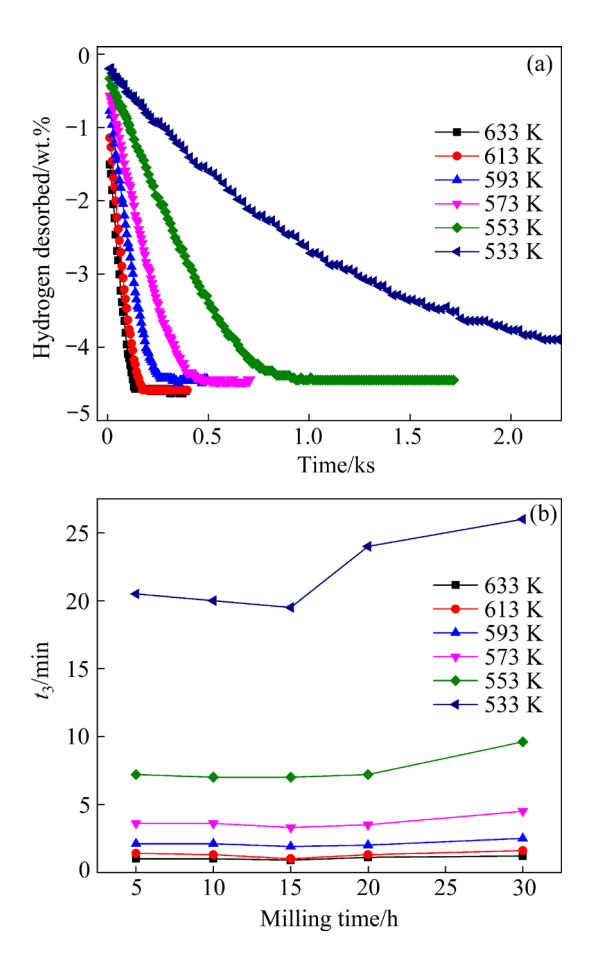


**Fig. 9** Hydrogen desorption curves of alloys at different temperatures: (a) Hydrogen desorption curves of  $M_{15}$  alloy; (b) Time needed for alloys to desorb 3 wt.% hydrogen ( $t_3$ )

which are very small and fluctuate a little when the temperature is above 573 K, as shown in Fig. 9(b). When the temperature decreases to 573 K and below, the  $t_3$  value increases rapidly and the difference resulting from changing milling time becomes more and more obvious. Taking 533 K as an example, the  $t_3$  value of the alloys milled for 5, 10, 15, 20 and 30 h is 20.5, 20.0, 19.5, 24.0 and 26.0 min, respectively. Apparently, the 15 h-milled alloy gets the optimal hydrogen desorption kinetics. Similar to the effect of ball milling on the hydrogen absorption kinetics as analyzed above, the positive influence of ball milling is resulted from the decreased grain size and the increased defect density, which can not only increase the specific surface area and shorten the path of hydrogen diffusion but also provide expressways for hydrogen diffusion and active sites for hydrogen composition and decomposition [41,42]. The negative influence of ball milling is related to the

too many amorphous phases which will block the hydrogen diffusion inside the alloys.

Apparent activation energy represents the lowest energy needed for a gas—solid reaction to occur. In this work, the apparent activation energy of the as-milled hydrogenated La<sub>1.7</sub>Y<sub>0.3</sub>Mg<sub>16</sub>Ni alloy for dehydrogenation reaction is assessed by the Arrhenius method. The hydrogen desorption reaction of Mg-based alloys is dominated by a nucleation and growth process [43], which can be modeled by the Johnson–Mehl–Avrami–Kolmogorov (JMAK) theory with the linear equation below [44]:

$$\ln[-\ln(1-\alpha)] = \eta \ln k + \eta \ln t \tag{10}$$

where t is the hydrogen desorption time,  $\alpha$  is the fraction of Mg transforming to MgH<sub>2</sub> at time t, k is the rate constant, and  $\eta$  is the Avrami exponent.

The JMAK plots of  $\ln[-\ln(1-\alpha)]$  vs  $\ln t$  at 553–633 K can be described with the data of hydrogen desorption curves, as presented in Fig. 10. The JMAK plots are almost linear, from the fitting lines of which the values of  $\eta$  and  $\eta \ln k$  at each temperature can be gained, and then the value of k could be gotten easily. The dehydrogenation activation energy ( $E_{\rm de}$ ) could be gained with the Arrhenius equation [45]:

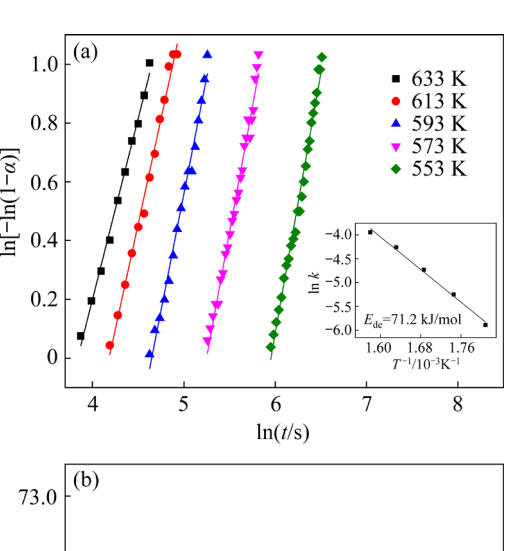
$$k = A \exp\left(\frac{-E_{\rm de}}{RT}\right) \tag{11}$$

where A represents a temperature-independent coefficient.

The Arrhenius plot of  $\ln k$  vs 1/T of the hydrogen desorption reaction of  $M_{15}$  alloy is linear, as shown in the inset of Fig. 10(a). The  $E_{de}$  value can be calculated from the slope of the fitting line of Arrhenius plot. Figure 10(b) shows the dependence of  $E_{de}$  value on milling time. Prolonging milling time from 5 to 30 h makes the  $E_{de}$  value decrease at first and increase later. The alloy milled for 15 h gets the lowest  $E_{de}$  value of 71.2 kJ/mol, which is lower than that of pure MgH<sub>2</sub> (~160 kJ/mol) [20], Mg<sub>17</sub>Ba<sub>2</sub> (173.9 kJ/mol) [46], MgH<sub>2</sub>–Li<sub>2</sub>TiO<sub>3</sub> (84 kJ/mol) [37] and MgH<sub>2</sub>–nfTa<sub>2</sub>O<sub>5</sub> (74 kJ/mol) [38], and is higher than that of Mg<sub>80</sub>Ce<sub>18</sub>Ni<sub>2</sub> (63 kJ/mol) [36].

During mechanical ball milling, the change of internal stress will lead to the deformation and fracture of the grains, forming an amorphous and nanocrystalline structure. When the nanocrystalline is much more than the amorphous phases, it is

conducive to the progress of desorbing hydrogen, and the dehydrogenation activation energy will be reduced. However, when the alloy is milled for too long time, it will contain too many amorphous phases, leading to an increase in the energy required for hydrogen diffusion, which is harmful to the hydrogen desorption reaction. Therefore, the dual regulation of the nanocrystalline and amorphous phases on the hydrogen storage kinetics results in the appearance of the lowest dehydrogenation activation energy. The value of  $E_{de}$  is an important index to assess the hydrogen desorption property by reflecting the energy barrier for releasing hydrogen from hydrides [47]. Thus, the reduced dehydrogenation activation energy resulting from mechanical milling is thought to be the real driving force of the enhancement of hydrogen desorption kinetics.



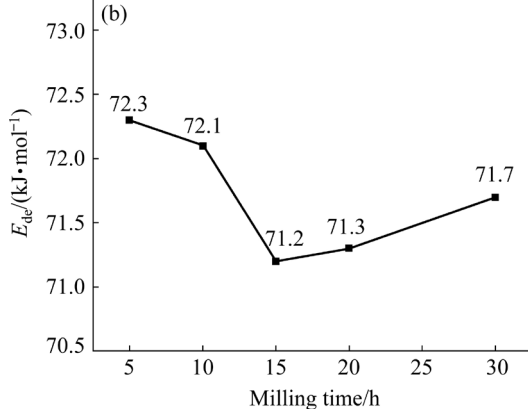


**Fig. 10** JMAK and Arrhenius plots, and  $E_{de}$  values of  $M_{15}$  alloys: (a) JMAK and Arrhenius plots; (b) Dependence of  $E_{de}$  value on milling time

#### **4 Conclusions**

(1) The  $La_{1.7}Y_{0.3}Mg_{16}Ni$  alloy contains an amorphous and nanocrystalline structure after ball

- milling. With extending milling time, the amorphous phase increases and the crystallinity, grain size and particle size decrease.
- (2) The thermodynamic parameter of alloys can be affected slightly by ball milling. The 15 h-milled alloy gets the minimal dehydrogenation enthalpy change of 72.9 kJ/mol.
- (3) Nanocrystalline and amorphous phases dually regulate the hydrogen storage kinetics of La<sub>1.7</sub>Y<sub>0.3</sub>Mg<sub>16</sub>Ni alloy. The 15 h-milled alloy has the optimal activation property, the fastest hydrogen absorption and desorption kinetics, and the smallest dehydrogenation activation energy of 71.2 kJ/mol.

#### **Acknowledgments**

This work is supported by the National Natural Science Foundation of China (Nos. 51731002, 51761032, 51871125).

#### References

- [1] WANG Yue, BISWAS A, RODRIGUEZ R, KESHAVARZ-MOTAMED Z, EMADI A. Hybrid electric vehicle specific engines: State-of-the-art review [J]. Energy Reports, 2022, 8: 832–851.
- [2] KUMAR A, MUTHUKUMAR P, SHARMA P, KUMAR E A. Absorption based solid state hydrogen storage system: A review [J]. Sustainable Energy Technologies and Assessments, 2022, 52: 102204.
- [3] TIAN Zhi-hui, WANG Ze-xuan, YAO Pu-fan, XIA Chao-qun, YANG Tai, LI Qiang. Hydrogen storage behaviors of magnesium hydride catalyzed by transition metal carbides [J]. International Journal of Hydrogen Energy, 2021, 46: 40203–40216.
- [4] YE Yang, YUE Yi, LU Jian-feng, DING Jing, WANG Wei-long, YAN Jin-yue. Enhanced hydrogen storage of a LaNi<sub>5</sub> based reactor by using phase change materials [J]. Renewable Energy, 2021, 180: 734–743.
- [5] OUYANG Liu-zhang, CHEN Wei, LIU Jiang-wen, FELDERHOFF M, WANG Hui, ZHU Min. Enhancing the regeneration process of consumed NaBH<sub>4</sub> for hydrogen storage [J]. Advanced Energy Materials, 2017, 7: 1700299.
- [6] ZHU Yong-yang, OUYANG Liu-zhang, ZHONG Hao, LIU Jiang-wen, WANG Hui, SHAO Huai-yu, HUANG Zhen-guo, ZHU Min. Closing the loop for hydrogen storage: Facile regeneration of NaBH<sub>4</sub> from its hydrolytic product [J]. Angewandte Chemie International Edition, 2020, 59: 8623–8629.
- [7] CHEN Kang, OUYANG Liu-zhang, ZHONG Hao, LIU Jiang-wen, WANG Hui, SHAO Huai-yu, ZHANG Yao, ZHU Min. Converting H<sup>+</sup> from coordinated water into H<sup>-</sup> enables super facile synthesis of LiBH<sub>4</sub> [J]. Green Chemistry, 2019, 21: 4380–4387.

- [8] LASS E A. Reversible hydrogen-storage at reduced temperatures in the intermetallic compound Mg<sub>6</sub>(Ni, Pd) [J]. International Journal of Hydrogen Energy, 2011, 36: 14496–14502.
- [9] ZHANG Xiao-yue, SUN Ya-hui, XIA Guang-lin, YU Xue-bin. Light-weight solid-state hydrogen storage materials characterized by neutron scattering [J]. Journal of Alloys and Compounds, 2022, 899: 163254.
- [10] LUO Qun, LI Jian-ding, LI Bo, LIU Bin, SHAO Huai-yu, LI Qian. Kinetics in Mg-based hydrogen storage materials: Enhancement and mechanism [J]. Journal of Magnesium and Alloys, 2019, 7: 58-71.
- [11] ZHANG Yang-huan, LI Long-wen, FENG Dian-chen, GONG Peng-fei, SHANG Hong-wei, GUO Shi-hai. Hydrogen storage behavior of nanocrystalline and amorphous La-Mg-Ni-based LaMg<sub>12</sub>-type alloys synthesized by mechanical milling [J]. Transactions of Nonferrous Metals Society of China, 2017, 27: 551–561.
- [12] CZUJKO T, VARIN R A, CHIU C, WRONSKI Z. Investigation of the hydrogen desorption properties of Mg + 10 wt.%X (X = V, Y, Zr) submicrocrystalline composites [J]. Journal of Alloys and Compounds, 2006, 414: 240–247.
- [13] ZHANG Jian, YAN Shuai, XIA Guang-lin, ZHOU Xiao-jie, LU Xian-zheng, YU Lin-ping, YU Xue-bin, PENG Ping. Stabilization of low-valence transition metal towards advanced catalytic effects on the hydrogen storage performance of magnesium hydride [J]. Journal of Magnesium and Alloys, 2021, 9: 647–657.
- [14] ZHONG Hai-chang, XU Jing-bo, JIANG Chun-hai, LU Xiang-jun. Microstructure and remarkably improved hydrogen storage properties of Mg2Ni alloys doped with metal elements of Al, Mn and Ti [J]. Transactions of Nonferrous Metals Society of China, 2018, 28: 2470–2477.
- [15] OUYANG L Z, YANG X S, DONG H W, ZHU M. Structure and hydrogen storage properties of Mg<sub>3</sub>Pr and Mg<sub>3</sub>PrNi<sub>0.1</sub> alloys [J]. Scripta Materialia, 2009, 61: 339–342.
- [16] OUYANG L Z, QIN F X, ZHU M. The hydrogen storage behavior of Mg<sub>3</sub>La and Mg<sub>3</sub>LaNi<sub>0.1</sub> [J]. Scripta Materialia, 2006, 55: 1075–1078.
- [17] PANDEY S K, BHATNAGAR A, SHUKLA V, KESARWANI R, DESHPANDEY U, YADAV T P. Catalytic mechanism of TiO<sub>2</sub> quantum dots on the de/re-hydrogenation characteristics of magnesium hydride [J]. International Journal of Hydrogen Energy, 2021, 46: 37340–37350.
- [18] YANG Li-li, LI Shu-jing, CHEN Jia-wen, LIU Jiang-chuan, ZHU Yun-feng, LIU Ya-na, ZHANG Ji-guang, QIAO Ya-jing, BA Zhi-xin, LI Li-quan. Significantly improved hydrogen storage properties of Mg90Al10 catalyzed by TiF3 [J]. Journal of Alloys and Compounds, 2022, 908: 164581.
- [19] OUYANG Liu-zhang, CAO Zhi-jie, WANG Hui, HU Ren-zhong, ZHU Min. Application of dielectric barrier discharge plasma-assisted milling in energy storage materials—A review [J]. Journal of Alloys and Compounds, 2017, 691: 422–435.
- [20] OUYANG L Z, CAO Z J, WANG H, LIU J W, SUN D L, ZHANG Q A, ZHU M. Enhanced dehydriding

- thermodynamics and kinetics in Mg(In)–MgF<sub>2</sub> composite directly synthesized by plasma milling [J]. Journal of Alloys and Compounds, 2014, 586: 113–117.
- [21] OUYANG L Z, CAO Z J, WANG H, LIU J W, SUN D L, ZHANG Q A, ZHU M. Dual-tuning effect of In on the thermodynamic and kinetic properties of Mg2Ni dehydrogenation [J]. International Journal of Hydrogen Energy, 2013, 38: 8881–8887.
- [22] MA Miao-lian, DUAN Ruo-ming, OUYANG Liu-zhang, ZHU Xiao-ke, CHEN Zhi-ling, PENG Cheng-hong, ZHU Min. Hydrogen storage and hydrogen generation properties of CaMgz-based alloys [J]. Journal of Alloys and Compounds, 2017, 691: 929–935.
- [23] ZHANG Wei, ZHAO Dong-liang, ZHANG Yang-huan, LI Jun, GUO Shi-hai, QI Yan, GAO Jin-liang. Effect of Y partially substituting La on the phase structure and hydrogen storage property of La–Mg–Ni alloys [J]. Journal of Physics and Chemistry of Solids, 2022, 167: 110744.
- [24] ZHANG Huai-wei, BAO Liang, PAN Ying, GE Jing-yuan. Enhanced hydrogen storage performances of binary Mg-Y nanoscale particles [J]. Chemical Physics Letters, 2022, 796: 139573.
- [25] ZHU M, WANG H, OUYANG L Z, ZENG M Q. Composite structure and hydrogen storage properties in Mg-base alloys [J]. International Journal of Hydrogen Energy, 2006, 31: 251–257.
- [26] MONTONE A, NOVAKOVIC J G, ANTISARI M V, BASSETTI A, BONETTI E, FIORINI A L, PASQUINI L, MIRENGHI L, ROTOLO P. Nano-micro MgH<sub>2</sub>-Mg<sub>2</sub>NiH<sub>4</sub> composites: Tayloring a multichannel system with selected hydrogen sorption properties [J]. International Journal of Hydrogen Energy, 2007, 32: 2926–2934.
- [27] YONG Hui, GUO Shi-hai, YUAN Ze-ming, QI Yan, ZHAO Dong-liang, ZHANG Yang-huan. Improved hydrogen storage kinetics and thermodynamics of RE-Mg-based alloy by co-doping Ce-Y [J]. International Journal of Hydrogen Energy, 2019, 44: 16765–16776.
- [28] HUEN P, PASKEVICIUS M, RICHTER B, RAVNSBAEK D B, JENSEN T R. Hydrogen storage stability of nanoconfined MgH<sub>2</sub> upon cycling [J]. Inorganics, 2017, 5: 57.
- [29] LIU Ya-na, ZOU Jian-xin, ZENG Xiao-qin, WU Xiao-mei, TIAN Hu-yong, DING Wen-jiang, WANG Jun. Study on hydrogen storage properties of Mg nanoparticles confined in carbon aerogels [J]. International Journal of Hydrogen Energy, 2013, 38: 5302–5308.
- [30] FRIEDRICHS O, SÁNCHEZ-LÓPEZ J C, LÓPEZ-CARTES C, DORNHEIM M, KLASSEN T, BORMANN R, FERNÁNDEZ A. Chemical and microstructural study of the oxygen passivation behaviour of nanocrystalline Mg and MgH<sub>2</sub> [J]. Applied Surface Science, 2006, 252: 2334–2345.
- [31] CHEN Xiao-wei, ZOU Wei-dong, LIN Qiu-bao, LI Ren-quan, XIA Guang-lin, YU Xue-bin. The effect of oxygen coverages on hydrogenation of Mg (0001) surface [J]. Applied Surface Science, 2019, 487: 510–518.
- [32] MENG Jie, PAN Yan-biao, LUO Qun, AN Xue-hui, LIU Yang, LI Qian, CHOU Kuo-chih. A comparative study on

- effect of microwave sintering and conventional sintering on properties of Nd-Mg-Ni-Fe<sub>3</sub>O<sub>4</sub> hydrogen storage alloy [J]. International Journal of Hydrogen Energy, 2010, 35: 8310-8316.
- [33] ZHANG Yang-huan, ZHANG Wei, YUAN Ze-ming, BU Wen-gang, QI Yan, DONG Xiao-ping, GUO Shi-hai. Hydrogen storage performances of as-milled REMg<sub>11</sub>Ni (RE=Y, Sm) alloys catalyzed by MoS<sub>2</sub> [J]. Transactions of Nonferrous Metals Society of China, 2018, 28: 1828–1837.
- [34] PASKEVICIUS M, SHEPPARD D A, BUCKLEY C E. Thermodynamic changes in mechanochemically synthesized magnesium hydride nanoparticles [J]. Journal of the American Chemical Society, 2010, 132: 5077–5083.
- [35] FRIEDLMEIER G, GROLL M. Experimental analysis and modelling of the hydriding kinetics of Ni-doped and pure Mg [J]. Journal of Alloys and Compounds, 1997, 253/254: 550–555
- [36] OUYANG L Z, YANG X S, ZHU M, LIU J W, DONG H W, SUN D L, ZOU J, YAO X D. Enhanced hydrogen storage kinetics and stability by synergistic effects of in situ formed CeH<sub>2.73</sub> and Ni in CeH<sub>2.73</sub>–MgH<sub>2</sub>–Ni nanocomposites [J]. The Journal of Physical Chemistry C, 2014, 118: 7808–7820.
- [37] ZHANG Teng-fei, ISOBE S, JAIN A, WANG Yong-ming, YAMAGUCHI S, MIYAOKA H, ICHIKAWA T, KOJIMA Y, HASHIMOTO N. Enhancement of hydrogen desorption kinetics in magnesium hydride by doping with lithium metatitanate [J]. Journal of Alloys and Compounds, 2017, 711: 400–405.
- [38] KUMAR S, TIWARI G P. Thermodynamics and kinetics of MgH<sub>2</sub>-nfTa<sub>2</sub>O<sub>5</sub> composite for reversible hydrogen storage application [J]. Journal of Materials Science, 2017, 52: 6962–6968.
- [39] SHAHI R R, BHATANAGAR A, PANDEY S K, SHUKLA V, YADAV T P, SHAZ M A, SRIVASTAVA O N. MgH<sub>2</sub>–ZrFe<sub>2</sub>H<sub>x</sub> nanocomposites for improved hydrogen storage characteristics of MgH<sub>2</sub> [J]. International Journal of Hydrogen Energy, 2015, 40: 11506–11513.
- [40] SCHLAPBACH L, ZÜTTEL A. Hydrogen-storage materials for mobile applications [J]. Nature, 2001, 414: 353–358.
- [41] YUAN Ze-ming, LI Xiao-ming, LI Tao, ZHAI Ting-ting, LIN Yong-hua, FENG Dian-chen, ZHANG Yang-huan. Improved hydrogen storage performances of nanocrystalline RE<sub>5</sub>Mg<sub>41</sub>-type alloy synthesized by ball milling [J]. Journal of Energy Storage, 2022, 46: 103702.
- [42] DARYANI M, SIMCHI A, SADATI M, HOSSEINI H M, TARGHOLIZADEH H, KHAKBIZ M. Effects of Ti-based catalysts on hydrogen desorption kinetics of nanostructured magnesium hydride [J]. International Journal of Hydrogen Energy, 2014, 39: 21007–21014.
- [43] ZOU Jian-xin, ZENG Xiao-qin, YING Yan-jun, CHEN Xi, GUO Hao, ZHOU Si, DING Wen-jiang. Study on the hydrogen storage properties of core-shell structured Mg-RE (RE = Nd, Gd, Er) nano-composites synthesized through arc plasma method [J]. International Journal of Hydrogen Energy, 2013, 38: 2337–2346.
- [44] AVRAMI M. Kinetics of phase change. Part III: Granulation, phase change and microstructure [J]. The Journal of

Chemical Physics, 1941, 9: 177-184.

- [45] YUAN Ze-ming, ZHANG Yang-huan, YANG Tai, BU Wen-gang, GUO Shi-hai, ZHAO Dong-liang. Microstructure and enhanced gaseous hydrogen storage behavior of CoS<sub>2</sub>catalyzed Sm<sub>5</sub>Mg<sub>41</sub> alloy [J]. Renewable Energy, 2018, 116: 878–891.
- [46] WU Dai-feng, OUYANG Liu-zhang, WU Cong, GU Qin-fen,
- WANG Hui, LIU Jiang-wen, ZHU Min. Phase transition and hydrogen storage properties of Mg<sub>17</sub>Ba<sub>2</sub> compound [J]. Journal of Alloys and Compounds, 2017, 690: 519–522.
- [47] FAN Mei-qiang, LIU Shu-sheng, ZHANG Yao, ZHANG Jian, SUN Li-xian, XU Fen. Superior hydrogen storage properties of MgH<sub>2</sub>-10wt.%TiC composite [J]. Energy, 2010, 35: 3417–3421.

### 球磨态 La-Y-Mg-Ni 合金的显微组织和储氢性能

张巍1,赵栋梁1,张羊换1,2,郭世海1,祁焱1

- 1. 钢铁研究总院 功能材料研究院, 北京 100081;
- 2. 内蒙古科技大学 白云鄂博共伴生矿资源高效综合利用省部共建协同创新中心,包头 014010

摘 要: 为了提高 La-Y-Mg-Ni 合金的储氢性能,通过对铸态合金进行 5~30 h 的球磨,制备具有非晶和纳米晶结构的 La<sub>1.7</sub>Y<sub>0.3</sub>Mg<sub>16</sub>Ni 合金,并研究显微组织对储氢性能的影响及其机理。结果表明,随着球磨时间的延长,合金的结晶度、晶粒尺寸和粒径减小,非晶相增加。纳米晶相和非晶相的双重调节作用导致储氢动力学性能先加快,后减慢。经过 15 h 球磨的合金具有最好的吸、放氢动力学特性,在 373 K 下 10 min 内可以吸收 3.10%(质量分数)的氢气,其放氢活化能最低,为 71.2 kJ/mol。球磨不同时间的合金的热力学性能的变化很小,球磨 15 h 后合金的放氢焓变最低,为 72.9 kJ/mol。

关键词: 镁基合金; 球磨; 显微组织; 晶粒细化; 纳米晶; 非晶相; 储氢动力学

(Edited by Wei-ping CHEN)